Experimental and numerical investigations of dike-break induced flows

S. Roger
Institute of Hydraulic Engineering and Water Resources Management (IWW), RWTH Aachen University, Hydraulic Laboratory, Kreuzherrenstr. 7, 52056 Aachen, Germany. Tel.: +(49) 241 80 93939; fax: +(49) 241 80 92275; E-Mail: roger@iww.rwth-aachen.de (author for correspondence)

B.J. Dewals, S. Erpicum, M. Pirotton
Unit of Hydrology, Applied Hydrodynamics and Hydraulic Constructions (HACH), Department ArGEnCo, University of Liege (ULg), Belgium (B.J. Dewals: also Fund for Scientific Research, F.R.S.-FNRS, Belgium), E-Mail: B.Dewals@ulg.ac.be, S.Erpicum@ulg.ac.be, Michel.Pirotton@ulg.ac.be

D. Schwanenberg
Deltares, Operational Water Management, Delft NL, E-Mail: dirk.schwanenberg@deltares.nl

H. Schüttrumpf, J. Köngeter
IWW, RWTH Aachen University, Germany, E-Mail: schuettrumpf@iww.rwth-aachen.de, koengeter@iww.rwth-aachen.de

Abstract Experimental model data are compared with numerical computations of dike-break induced flows, focusing on the final steady state. An idealised scale model was designed reproducing the specific boundary conditions of dike breaks. Discharges, water levels and depth profiles of horizontal velocities were recorded and validated by numerical modeling. The latter was performed by two different models solving the two-dimensional depth-averaged shallow water equations, namely a total variation diminishing Runge-Kutta discontinuous Galerkin finite element method, and a finite volume scheme involving a flux vector splitting approach. The results confirmed convergence and general applicability of both methods for dike-break problems. As regards their accuracy, the basic flow pattern was satisfactorily reproduced yet with differences compared to the measurements. Hence, additional simulations by a finite volume model were performed considering various turbulence closures, wall-roughnesses as well as non-uniform Boussinesq coefficients.

1. Introduction

1.1 *Motivation*

Dikes or (mobile) walls are essential parts of flood protection conceptions along river banks to protect densely populated areas from flooding. Massive flood events and recurring dike failures indicate that inland flood protection systems may be vulnerable. The assessment of this risk involves the identification of inundated areas as well as flow depths and velocities of the initiated wave. In this context, the discharge through the breach of a collapsed dike section significantly affects the final water level and its rising speed in the floodplain.

The static impact for a slow increase of the water level in a floodplain basically depends on the total water volume entering the floodplain over a long period, while during the first transient phase of a dike break, flow velocities and water depths within the flood wave induce dynamic damages nearby the breach. Compared to the duration of the whole event this period is often short but equally dangerous for people and property.

Beside the damage calculation in a risk assessment procedure, the results of flood wave computations are used to manage the residual risk. The definition of evacuation zones, the coordination of civil protection and emergency measures as well as the land use planning are important for risk mitigation. The simulation of various scenarios may provide authorities with valuable information in terms of flood arrival time and main flow directions. Additional applications include the design and risk analysis of mobile flood protection systems in combination with the determination of safety areas. Insurance companies also have an interest in modifying their computational approaches as regards damage categories. Moreover, there are European legal attempts to identify and to illustrate areas with a significant flood risk.

1.2 *Phenomenon and procedure*

The wide knowledge concerning dam-break waves (CADAM 2000, IMPACT 2005) cannot directly be transferred to dike-break induced flows. The latter are influenced by the momentum component parallel to the protection structure causing asymmetric flood wave propagation. Moreover, unlike reservoirs at rest, a river bed will not be empty, but the persisting flood discharge leads to a fixed water level in the breach as the final steady state is approached resulting in a partition of the inflow into the downstream and the breach discharges (Fig. 1). This state has to be considered when focusing the long-term inundation and the resulting static impact in the entire floodplain. There is a lack of knowledge as regards these types of flood waves. The existing measured data are not sufficient due to the unpredictability and the danger of such events.

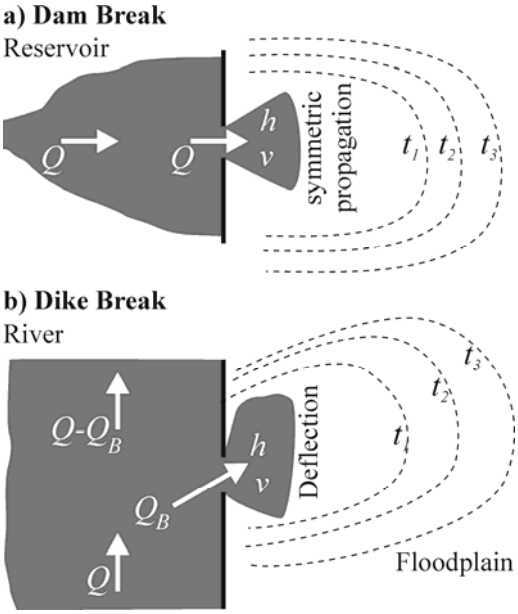

Figure 1 (a) Dam-break versus (b) dike-break induced flow

There exist only few investigations considering the propagation of a wave into an area, such as Fraccarollo and Toro (1995) or Kulisch (2003), relating to dam-break flows, however. Aureli and Mignosa (2002, 2004) only considered the presence of a permanent river discharge.

Circumventing the expense of a full-sized prototype, a bench-scale model was used to provide experimental data, which were recorded with sophisticated measurement techniques to explore flow effects and to validate numerical models. Physical and numerical models were combined in a hybrid approach. On the one hand, the accuracy of numerical forecasts was quantified by measurements. On the other hand, numerical simulations complement the model tests by calculating scenarios of different configurations, geometries and boundary conditions. Hence, this combination enables selective improvements in numerical methods and more reliable forecasts for long-term and large-scale applications. The experimental and numerical parts of this research are detailed in section 2. The mathematical model is presented in section 3, while its numerical implementation in two distinct simulation models follows in section 4. Section 5 highlights the ability of both models to represent the main characteristics of dike-break induced flows under four different hydraulic conditions. Next, the measurements are compared with additional results obtained with the finite volume model, taking into consideration different turbulence closures, wall roughness and Boussinesq coefficients. Finally, conclusions are drawn.

2. Scale model tests

2.1 *Apparatus and idealised experimental set-up*

The model shown in Fig. 2 was designed taking into account the special boundary conditions of a dike-break induced flow close to the breach section (Briechle et al. 2004, Briechle 2006). It consists of a 1 m wide horizontal channel with a pneumatically driven gate at one bank and a 3.5×4.0 m^2 adjacent propagation area made of glass. A complete gate opening takes less than 0.3 s, representing the worst case scenario of a sudden and total dike failure. Moreover, the opening mechanism is a combination of pull and rotation to minimize effects on the free water column as the wave is initiated.

In contrast to flumes, the water propagates radially and falls off the glass plate freely at three sides. The bottom of the propagation area is made of glass to enable laser measurements from below the plate. Initial channel water levels were 0.3 to 0.5 m, channel discharges 0.1 to 0.3 m^3/s, and breach widths between 0.3 and 0.7 m.

2.2 *Measuring techniques*

As regards the boundary conditions, the inflow was controlled via an ultrasonic flow-measuring device. A weir at the channel end was calibrated for different crest heights to control the initial water depth. The steady-state breach discharge Q_B was indirectly calculated as the difference between the model inflow and the weir overflow Q_w. Due to strong spatial variations of the initiated wave and air entrainment, an advanced non-intrusive measuring techniques was necessary, providing high frequency and stability towards highly unsteady water levels.

Thus, water depths were recorded by ultrasonic sensors with 25 Hz frequency all over the propagation area with grid lengths of $\Delta x = \Delta y = 0.2$ m, and a refined grid of 0.1 m close to the breach zone. Within the channel, the detection was performed at various cross-sections, again using a higher resolution up to 0.5 m from the breach section. The sensors were mounted on movable cross-beams enabling measurements at various locations. Despite the steep wave front at some locations, errors were usually less than ±2 mm because the adopted sensors have an operating range of 0.35 m for the small detection zone considered with 0.18 mm resolution. Detections at each grid point consisted of 500 single values which were statistically evaluated, and the test reproducibility was also checked. Up to eight sensors were used simultaneously. Mean depth-averaged velocity profiles $u(z)$, $v(z)$ were sampled using a conventional 1D Laser-Doppler Anemometer (LDA), mounted on an automatic traversing unit beneath the glass plate. At the three cross-sections $y = 0.25$, 0.30, 0.35 m near the breach the depth-averaged velocity components were measured in using a denser grid of $\Delta x = 0.05$ m, $\Delta z = 0.01$ m within the wave.

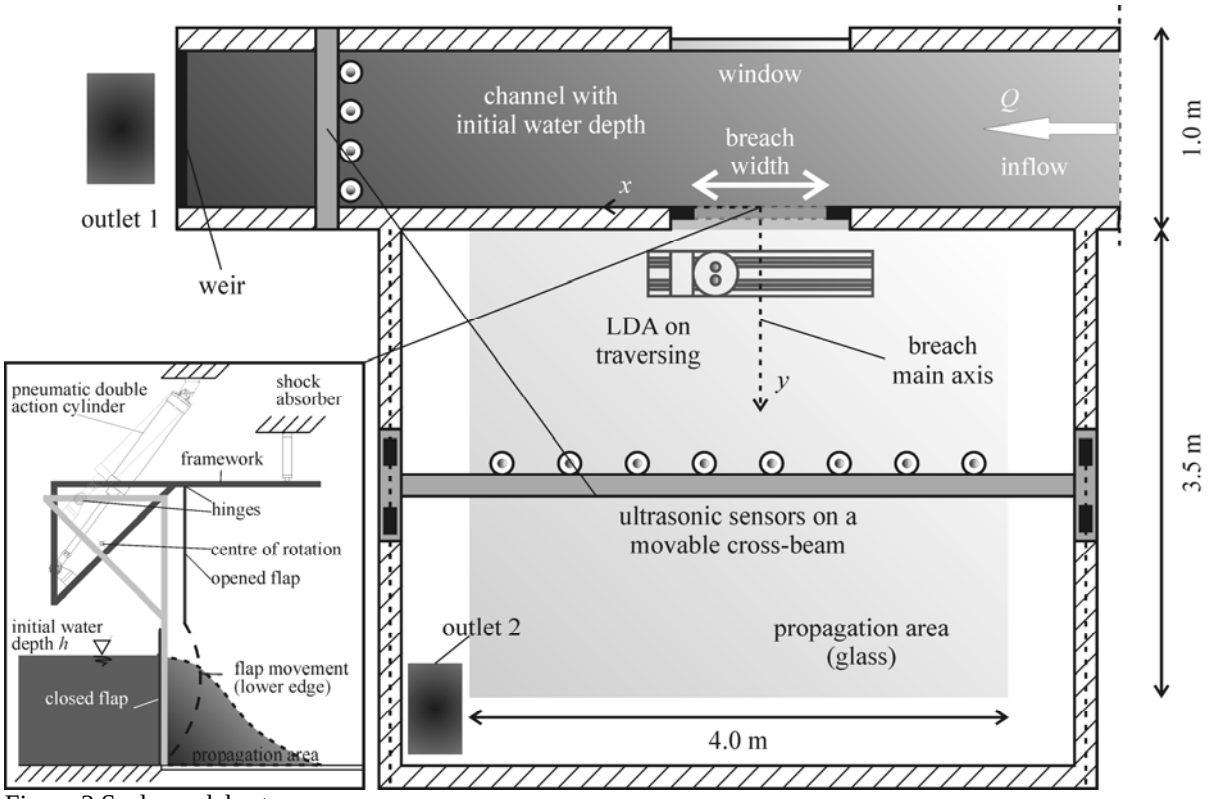

Figure 2 Scale model set-up

3. Mathematical model

3.1 *Governing equations*

Both models are based on the 2D depth-averaged equations of mass and momentum conservation, referred to as the Shallow-Water Equations (SWE). The basic assumption states that velocities normal to the main flow directions remain small. As a consequence the pressure field is hydrostatic, which may limit the applicability of the SWE. Their conservative form can be written as follows, using vector notation

$$\partial_t \mathbf{s} + \partial_x \mathbf{f} + \partial_y \mathbf{g} + \partial_x \mathbf{f}_d + \partial_y \mathbf{g}_d = \mathbf{S}_o - \mathbf{S}_f \,, \tag{1}$$

$$\mathbf{s} = \begin{pmatrix} h \\ hu \\ hv \end{pmatrix}, \quad \mathbf{S}_o = \begin{pmatrix} 0 \\ \partial_x z_b \\ \partial_y z_b \end{pmatrix}, \quad \mathbf{S}_f = \begin{pmatrix} 0 \\ \tau_{bx}/\rho \\ \tau_{by}/\rho \end{pmatrix}, \tag{2}$$

$$\mathbf{f} = \begin{pmatrix} hu \\ \rho_{xx} hu^2 + \frac{1}{2} g h^2 \\ \rho_{xy} huv \end{pmatrix}, \qquad \mathbf{f}_d = -\frac{h}{\rho} \begin{pmatrix} 0 \\ \sigma_x \\ \tau_{xy} \end{pmatrix}, \tag{3}$$

$$\mathbf{g} = \begin{pmatrix} hv \\ \rho_{xy} huv \\ \rho_{yy} hv^2 + \frac{1}{2} g h^2 \end{pmatrix}, \qquad \mathbf{g}_d = -\frac{h}{\rho} \begin{pmatrix} 0 \\ \tau_{xy} \\ \sigma_y \end{pmatrix} \tag{4}$$

where $\mathbf{s}$ = vector of conservative unknowns, t = time, $\mathbf{f}$, $\mathbf{g}$ = advective and pressure fluxes in directions x and y, $\mathbf{f}_d$, $\mathbf{g}_d$ = diffusive fluxes, $\mathbf{S}_o$ = bottom slope, $\mathbf{S}_f$ = friction slope, h = flow depth, u, v = depth-averaged velocity components in x- and y-directions, z_b = bottom elevation, g = gravitational acceleration, ρ = water density, τ_{bx} , τ_{by} = bottom shear stresses, and σ_x, σ_y, τ_{xy} = turbulent stresses. The Boussinesq coefficients ρ_{xx}, ρ_{yy}, ρ_{xy} account for uneven distributed local flow velocities $\hat{u}$, $\hat{v}$ over the flow depth with angle brackets representing depth-averaging, namely

$$\begin{aligned} &\rho_{xx} = \left\langle \hat{u}^2 \right\rangle / u^2 \geq 1 \quad \text{and} \quad \rho_{yy} = \left\langle \hat{v}^2 \right\rangle / v^2 \geq 1 \\ &\rho_{xy} = \left\langle \hat{u}\hat{v} \right\rangle / uv, \qquad \rho_{xy}^2 \leq \rho_{xx}\rho_{yy} \end{aligned} \tag{5}$$

3.2 *Closure relations*

The bottom friction is conventionally modeled using an empirical law, such as the Manning formula. The models enable the definition of a spatially distributed roughness coefficient. Besides, the finite volume model provides the additional possibility to reproduce friction along the side walls by means of a process-oriented formulation (Dewals 2006, Dewals et al. 2008) as

$$\begin{aligned} \frac{\tau_{bx}}{\rho g h} &= u \left[\sqrt{u^2 + v^2}\, \frac{n_b^2}{h^{4/3}} + \sum_{k_x=1}^{N_x} \frac{4}{3} \frac{u_{k_x} n_w^2}{h_{k_x}^{1/3} \Delta y} \right] \\ \frac{\tau_{by}}{\rho g h} &= v \left[\sqrt{u^2 + v^2}\, \frac{n_b^2}{h^{4/3}} + \sum_{k_y=1}^{N_y} \frac{4}{3} \frac{v_{k_y} n_w^{3/2}}{h_{k_y}^{1/3} \Delta x} \right] \end{aligned} \tag{6}$$

where the Manning coefficients n_b and n_w (s/m$^{1/3}$) characterize bottom and side-wall roughnesses, respectively. N_x and N_y designate the number of edges of the finite volume cell which are in contact with the side-wall.

The turbulent stresses are expressed following the Boussinesq approximation (ASCE 1988, Rodi 1984)

$$\sigma_x = 2\rho(\nu+\nu_T)\partial_x u,\ \sigma_y = 2\rho(\nu+\nu_T)\partial_y v,$$
$$\tau_{xy} = \tau_{yx} = (\nu+\nu_T)\rho(\partial_y u + \partial_x v),\ (\nu \ll \nu_T) \quad (7)$$

where ν_t = depth-averaged turbulent eddy viscosity, and ν = molecular kinematic viscosity.

4. Computational models

The mathematical model described above was implemented within two different computational models of which Table 1 details the main characteristics.

Table 1 Comparison of FE model versus FV model

	FE model	FV model
Model name	DGFlow	WOLF 2D
Model type	Finite Element	Finite Volume
Space discretization	Discontinuous Galerkin (DG)	Flux Vector Splitting (FVS)
Time integration	TVD Runge-Kutta	Runge-Kutta
Grid	Triangular	Cartesian
Turbulence closure	None	Algebraic/k-ε
Wall roughness	None	Accounted for
Boussinesq coefficients	Set to unity	Distributed values

4.1 *Finite element model* (*FE model*): *DGFlow*

DGFlow is based on the Runge-Kutta discontinuous Galerkin (RKDG) method for hyperbolic equation systems and the local discontinuous Galerkin method for advection-dominated flows (Cockburn 1999, Cockburn et al. 2000). The leadoff implementation of the RKDG method to the SWE was presented by Schwanenberg and Köngeter (2000). Schwanenberg and Harms (2002, 2004) gave first applications to dam-break flows and developed the Total Variation Diminishing (TVD) RKDG finite element method, which is frequently applied at IWW, RWTH Aachen University. The scheme can be divided into three main steps:

- DG space discretization with a polynomial degree k decouples the partial differential equation into a set of ordinary differential equations,
- Ordinary differential equations are integrated in time by a (k+1)-order TVD RK method, and
- Slope limiter is applied on every intermediate time step.

The scheme is well suited to handle complicated geometries and requires only a simple treatment of boundary conditions and source terms to obtain high-order accuracy and sharp representation of shocks. By using orthogonal shape functions the resulting mass matrix becomes diagonal. Together with the explicit time integration, RKDG is computationally as efficient for transcritical, convection-dominated shallow water flows on unstructured 2D grids as comparable state-of-the-art finite volume schemes (Shu 2003). Furthermore, the computation of a numerical flux at the intercell boundaries introduces up-winding into the scheme while keeping the Galerkin test function inside the element. A slope limiter guarantees stability at shock zones by introducing a selective amount of dissipation for pure hyperbolic problems.

A detailed presentation as regards the space and time discretization, the approximation of the numerical flux for the DG method and the description of the slope limiter were presented by Schwanenberg (2003) and Schwanenberg and Harms (2004). As yet, the current model version has mainly been applied to dam-break flows. Therefore, viscous effects are neglected compared to the convective transport in the main direction. Moreover, the momentum correction coefficients are set to unity, i.e.

$$\mathbf{f}_d = \mathbf{g}_d = 0 \quad \text{and} \quad \rho_{xx} = \rho_{xy} = \rho_{xy} = 1 \quad (8)$$

The effects of these simplifications as regards dike-break induced flows are analyzed with the FV model described below.

4.2 *Finite volume model* (*FV model*): *WOLF 2D*

The depth-averaged flow model WOLF 2D was developed at the University of Liege for about a decade. It includes a mesh generator and deals with multi-block Cartesian grids. This feature increases the size of possible simulation domains and enables local mesh refinements close to interesting areas, while preserving lower computational cost required by Cartesian compared to unstructured grids. A grid adaptation technique restricts the simulation domain to the wet cells. The space discretization of the divergence form of Eq. (1) is performed by means of a Finite Volume scheme (FV). Variable reconstruction at cells interfaces is either constant or linear, combined with a slope limiter, leading in the latter case to 2nd-order space accuracy.

Appropriate flux computation has always been a challenging issue in finite volume schemes. Herein, the fluxes **f** and **g** were computed by a Flux Vector Splitting (FVS) method developed by HACH, University of Liege. Following this FVS, the up-winding direction of each flux term **f** and **g** is simply dictated by the sign of the flow velocity reconstructed at the cell interfaces. A “von Neumann” stability analysis has demonstrated that FVS then leads to a stable spatial discretization of the gradients **f** and **g** in Eq. (1) (Dewals 2006). Besides requiring low computational cost, this FVS offers the advantages of being completely Froude-independent and of facilitating a satisfactory adequacy with the discretization of the bottom slope term. This FVS has already proven its validity and efficiency for numerous applications (Dewals 2006, Dewals et al. 2006a, b, 2008, Erpicum 2006, Erpicum et al. 2007).

Due to their diffusive nature, the fluxes $\mathbf{f}_d$ and $\mathbf{g}_d$ are legitimately evaluated by means of a centred scheme.

Since the model is applied to compute steady-state solutions, the time integration is performed by means of a 3-step first-order accurate Runge-Kutta algorithm, providing adequate dissipation in time. For stability reasons, the time step was constrained by the Courant-Friedrichs-Levy (CFL) condition based on gravity waves. A semi-implicit treatment of the bottom friction term in Eq. (6) was used, without requiring additional computational cost.

Besides, wetting and drying of cells is handled free of volume and momentum conservation error by means of an iterative resolution of the continuity equation at each time step (Erpicum 2006). A four-step procedure was followed at each temporal step integration:

1. Continuity equation is evaluated,
2. Algorithm detects cells with a negative flow depth to reduce the outflow unit discharge such that the computed water depth in these cells is strictly equal to zero,
3. Since these flux corrections may induce the drying in cascade of neighbouring cells, steps 1 to 3 are repeated iteratively, and
4. Momentum equations are computed based on the corrected unit discharge values.

In most practical applications, no more than two iterations are necessary, keeping thus the computation cost limited.

Several turbulence models are implemented in the FV model, starting from simple algebraic expressions of turbulent viscosity, to a depth-integrated model involving additional partial differential equations. Two different approaches were compared herein (see 5.5). First, a simple algebraic turbulence closure was adopted, assuming that turbulence is bed-dominated, for which turbulent kinematic viscosity may be expressed with $\alpha \approx 0.5$ (Fisher et al. 1979) as

$$\nu_T = \alpha h u_*, \tag{9}$$

and friction velocity u_* defined as (Ghamry and Steffler 2002)

$$u_*^2 = \sqrt{\tau_{bx}^2 + \tau_{by}^2} \Big/ \rho \tag{10}$$

Second, a depth-averaged k-ε model with two different length-scales accounting for vertical and horizontal turbulence mixing was applied, as developed by Erpicum (2006).

4.3 *Boundary conditions*

In both computational models, the value of the specific discharge can be prescribed as an inflow boundary condition. Besides, the transverse specific inflow discharge is usually set to zero. The outflow boundary condition may be a water surface elevation, a Froude number or no specific condition if the outflow is supercritical. At solid walls, the component of the specific discharge normal to it was set to zero.

In the FV model, to evaluate the diffusive terms, the gradients of the unknowns in the direction parallel to the boundary were set to zero for simplicity, while the gradients of the variables in the direction normal to the boundary were properly evaluated by finite differences between the boundary value and the centre value of the adjacent cell (Erpicum 2006). Regarding turbulence variables, the law of the wall was used to compute shear velocity on solid walls to determine the corresponding depth-averaged turbulent kinetic energy and its dissipation rate (Rodi 1984, Younus and Chaudhry 1994). At inlets, the turbulent kinetic energy and its dissipation rate were also prescribed (Choi and Garcia 2002, Ferziger and Peric 2002).

5. Numerical tests and results

5.1 *Computational procedure and grid*

Although the present analysis explicitly focused on steady state conditions, both computational models were run starting from an initial condition corresponding to steady channel flow. The whole transient propagation and development of the dike break wave has been simulated until the final steady solution was achieved.

The Cartesian grid used in the FV model involved almost 60,000 cells 0.02 m by 0.02 m. In contrast, the FE model simulations based upon about 23,000 triangular cells and 12,000 discrete nodes, with an average element edge length of 0.05 m. Nearby the breach, local grid refinement was used resulting in 0.03 m edges. After describing below the various tested configurations as well as the corresponding boundary conditions, the following subsections successively include base simulations, effects of 2nd order space discretization, turbulence modelling, bed and wall friction as well as Boussinesq coefficients.

5.2 *Test configurations*

Four different initial hydraulic configurations were considered, depending on the inflow discharge and the initial channel flow depth. Before each model run, a steady flow was established in the channel with the corresponding initial flow depth. Preferably high values of the flow depth were adopted to result in high values of downstream and breach discharges after the flow split, to obtain moderate velocities in the channel. Table 2 defines each of these configurations. At the channel inlet (Fig. 2), the unit discharge was prescribed as an upstream boundary condition. At the edges of the propagation area (glass plate) no

boundary condition was needed for supercritical outflow.

Calibrated weir formulas for various crest heights (Table 2) were implemented in both codes as possible downstream boundary conditions. Thus, the dynamics of the weir discharge depending on the actual channel water level could be modelled. The resulting backwater effects and flow resistances interact with the flow split into breach discharge and downstream channel discharge. The rating curve of each of those weirs was determined experimentally using a variable discharge coefficient as

$$Q_w = \frac{2}{3}\mu\, b\sqrt{2g}\,(h-h_w)^{3/2} = \frac{2}{3}\mu\sqrt{2g}\,h_0^{3/2} \qquad (11)$$

where Q_w = weir discharge, μ = discharge coefficient, b = crest width = 1.0 m, h = upstream water depth, h_w = crest height and $h_0 = h - h_w$ as overflow depth. The discharge coefficient measured experimentally was expressed as a cubic polynomial of h_0 (Table 3)

$$\mu = a_3 h_0^3 + a_2 h_0^2 + a_1 h_0 + a_0 \qquad (12)$$

Table 2 Definition of test configurations in numerical simulations for breach width = 0.70 m

Test ID	Inflow discharge [m^3/s]	Initial depth [m]	Crest height [m]
Q300-h50	0.300	0.50	0.241
Q300-h40	0.300	0.40	0.152
Q200-h50	0.200	0.50	0.297
Q200-h40	0.200	0.40	0.202

Table 3 Coefficients of cubic approximations

Test ID	a_3	a_2	a_1	a_0	Range of validity
Q300-h50	–7.291	4.561	–0.554	0.752	$0.05 < Q < 0.3$
Q300-h40	–10.84	6.009	–0.359	0.738	$0.05 < Q < 0.3$
Q200-h50	–62.63	26.61	–3.508	0.887	$0.03 < Q < 0.2$
Q200-h40	–65.62	29.01	–3.665	0.877	$0.03 < Q < 0.2$

5.3 *Base simulations*: *2nd order accurate space discretization with FE model and FV model*

Figures 3 and 4 show the global flow pattern of the deviated flood wave, respectively in terms of flow depths, unit discharge and wave deflection computed for test Q300-h50. The Froude numbers (Fig. 5), defined as $F = (u^2+v^2)^{1/2} / (gh)^{1/2}$, indicate a distinctive S-shaped critical section across the breach. The contour lines of wave heights confirm the influence of momentum of the channel main flow direction.

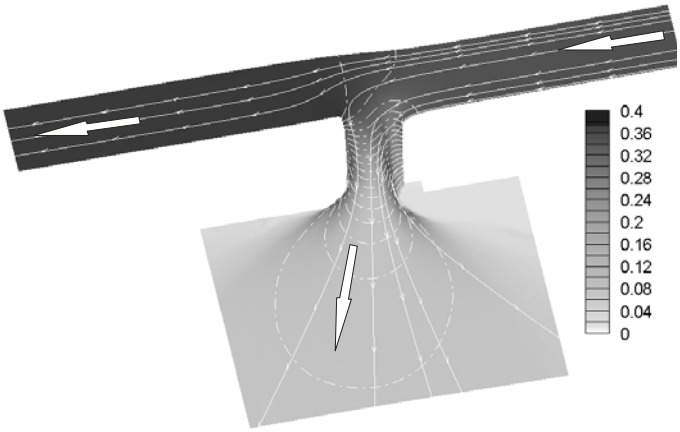

Figure 3 Deflection of wave (dash-dotted contours), stream traces and flow depth [m] computed with FE model

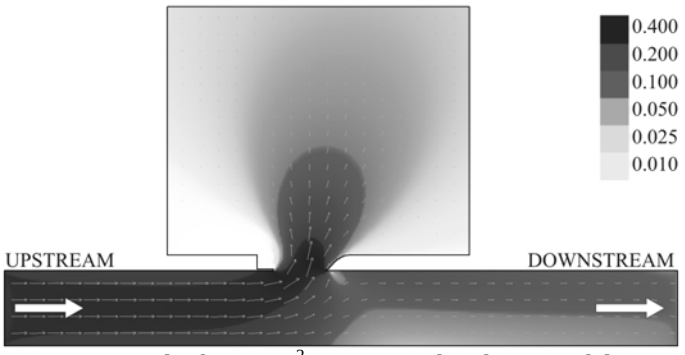

Figure 4. Unit discharge [m^2/s] computed with FV model

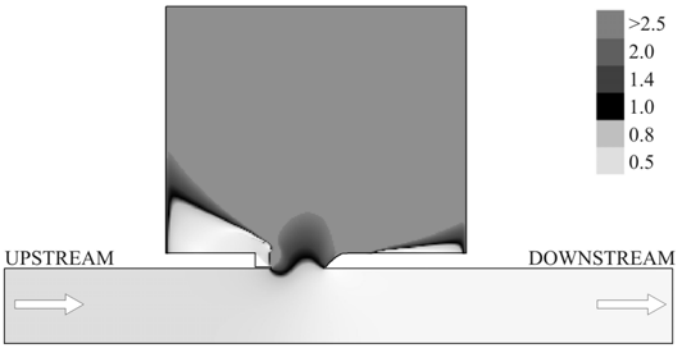

Figure 5 Froude number [-] computed with FV model

Flow depths predicted by the two computational models are compared with the values observed experimentally along the main y-axis at $x = 0$ in Fig. 6. As shown by the error bars, the range of uncertainty of the experimental measures is strongly influenced by the free surface inclination. The simulation results of both computational models are globally in satisfactory agreement with the observations. Figure 6 shows however some discrepancies in zones where the free surface curvature is significant. Besides, the results of both numerical models agree remarkably well, despite of their differences in terms of computational implementation (Table 1).

Simulated and measured discharges across the breach are compared in Table 3 and Fig. 7. For all four tests the numerical predictions underestimate the discharge released into the floodplain by 6 to 11% of the test breach discharge. The next sections aim at investigating whether this issue can be enhanced in the framework of depth-averaged flow modelling.

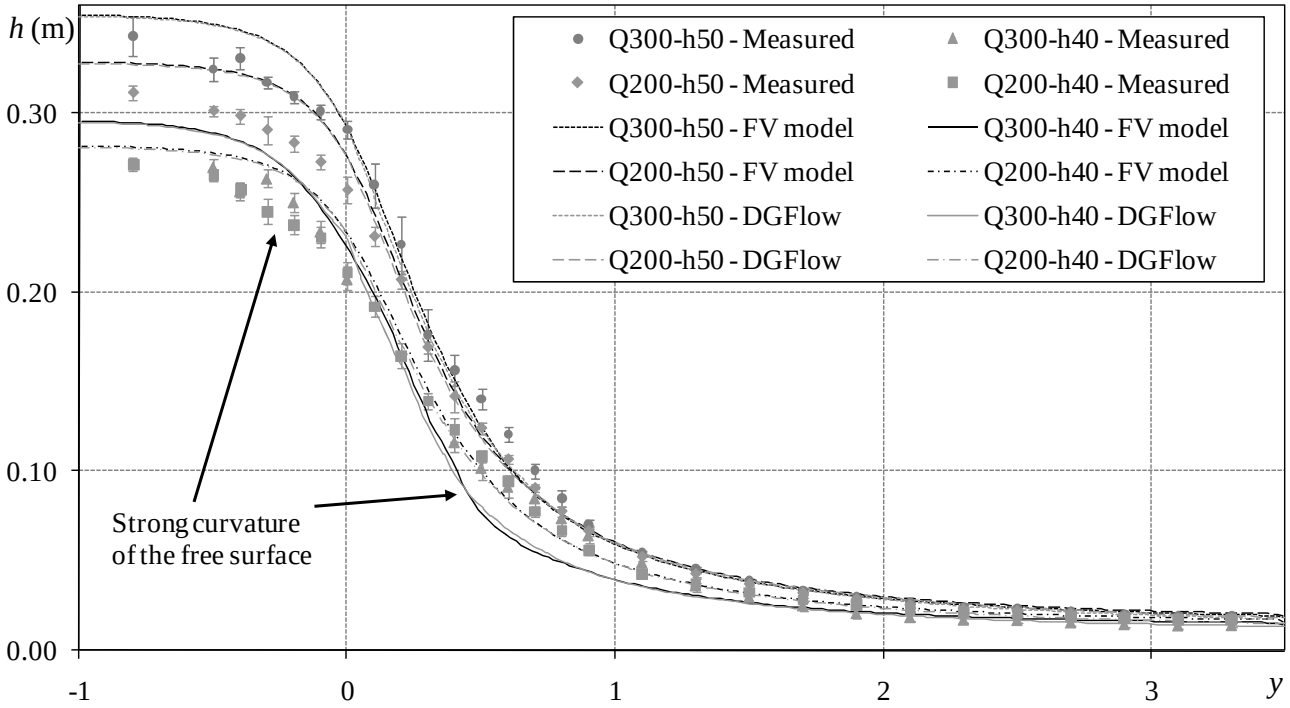

Figure 6 Surface profiles along y-axis at $x = 0$ (Fig. 2): Comparison of experimental and numerical results of base simulations (FE and FV models)

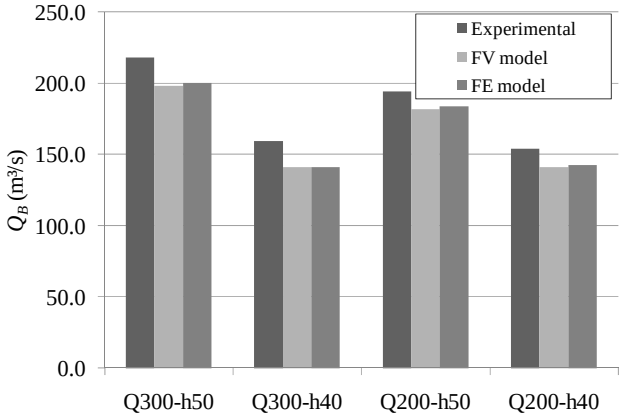

Figure 7 Comparison between breach discharges Q_B observed and computed by 2nd order accurate simulations

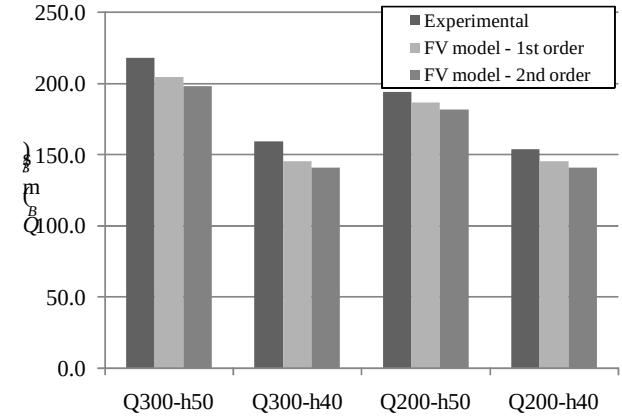

Figure 8 Comparison of experimental and numerically predicted (1st and 2nd order space discretization) breach discharges Q_B

Table 3 Comparison between breach discharges observed and computed with 2nd order accuracy by both models

Test ID	Measured [m³/s]	FE model [m³/s]	FV model [m³/s]
Q300-h50	0.218	0.200	0.198
Q300-h40	0.159	0.141	0.141
Q200-h50	0.194	0.183	0.182
Q200-h40	0.154	0.143	0.141

5.4 *Influence of space discretization*

Simulations of 1st order accuracy in space were conducted with the FV model. Figure 8 and Table 4 show that the predicted breach discharge is increased in the 1st order space accurate simulations compared to 2nd order. The numerical diffusive effects act thus favourably on the simulation results, but may not be considered as reliable since this diffusion strongly depends on purely numerical parameters, such as grid size. Therefore, the following simulations were run with 2nd order space discretization and a turbulence closure was added to represent the effect of real physical diffusion.

A preliminary study with the FE model yielded the required fineness of the numerical grid to obtain an almost mesh-independent solution and to minimize the discretization error (Fig. 9). Following Ferziger and Peric (1996) for unstructured grids, coarse grid results were interpolated on a fine grid to form the error estimate. In comparison to a very fine mesh, the averaged water level difference for each 0.02 m cell decreases for each uniform refinement. The selected locally refined grid consists of only 23,000 triangular elements and in parallel achieves a high accuracy.

Table 4 Comparison of experimental and numerical (FV model with 1st and 2nd order space accuracy) breach discharges

Test ID	Measured [m³/s]	1st order [m³/s]	2nd order [m³/s]
Q300-h50	0.218	0.204	0.198
Q300-h40	0.159	0.145	0.141
Q200-h50	0.194	0.186	0.182
Q200-h40	0.154	0.145	0.141

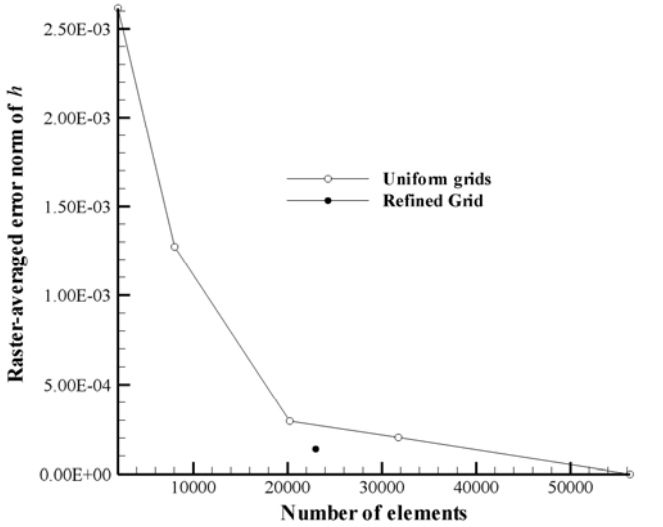

Figure 9 Grid refinement study computed with FE model for test configuration Q300-h50

5.5 *Influence of turbulence modelling*

The simulations were repeated with two types of turbulence closures (4.2), the first being a purely algebraic expression for eddy viscosity, involving parameter α from Eq. 9. Two different values were used to appreciate the sensitivity of the computed discharge with respect to α. The second is a two-equation depth-averaged k-ε model.

Table 5 Simulations performed with different turbulence closures (FV model). Relative change in breach discharge (%) compared to simulations without turbulence closure

Test ID	k-ε	Eq. (9) $\alpha = 0.5$	Eq. (9) $\alpha = 1.0$
Q300-h50	0.0	1.1	1.7
Q300-h40	0.0	2.7	4.7
Q200-h50	–0.1	0.7	0.8
Q200-h40	–0.1	0.7	1.3

As summarized in Table 5 and in Fig. 10, the turbulence closure has basically a minor effect on the computational results, most probably as a result of the highly advective nature of dike break induced flow. In such conditions, the pressure gradients and the purely advective terms in the momentum equations dominate diffusion, which only plays a minor role. In particular the effect of the k-ε turbulence closure on breach discharge is negligible, while the algebraic closure was run with slightly overestimated values of α to appreciate the relative sensitivity of the four test configurations with respect to the turbulence closure.

As regards the algebraic turbulence closure, Table 5 also shows that the discharge in test Q300-h40 is the most sensitive to the turbulence closure. Indeed, the velocity is maximum with a high inflow and a comparatively low initial flow depth, and hence so are the bottom shear stress and the friction velocity, directly controlling the magnitude of the eddy viscosity. In contrast, the sensitivity of the result is found minimal in test Q200-h50, for which the flow velocity is also small with a low inflow discharge and a high initial water depth.

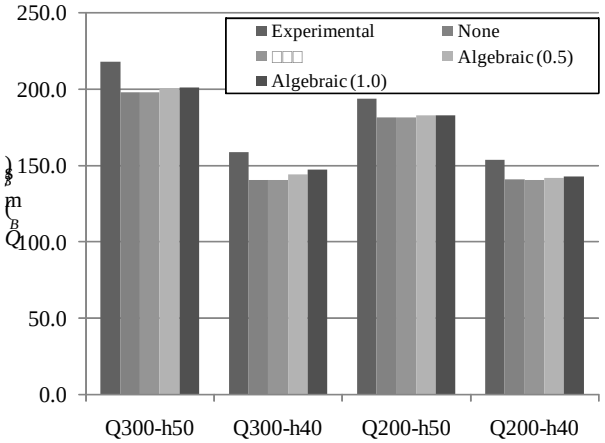

Figure 10 Comparison between breach discharges observed experimentally and predicted by 2nd order accurate simulations of FV model with various turbulence closures Q_B

Since the equations of motion, in particular the k-ε turbulence closure, are transport equations, proper boundary conditions need to be prescribed notably at the inlet and possibly influence the computational result further downstream in the simulation domain. Therefore, the sensitivity of the simulation output with respect to the length of the inlet channel was investigated. Therefore, two simulations (with and without k-ε turbulence closure) were repeated for test Q300-h50 with a length of the inlet channel increased by 10 m (Fig. 11). The flow remains essentially insensitive to the inlet channel length, since the variation in breach discharge does not exceed 0.2%.

Figure 11 Unit discharge [m²/s] computed with FV model for test Q300-h50 with an elongated inflow channel

5.6 *Influence of bed and wall roughness*

It has been verified with both computational models that modifying the Manning coefficient for a channel bed roughness within $0.005 < n_b < 0.020$ s/m$^{1/3}$ has no significant effect on the breach discharge (0.3%). Increasing the Manning coefficient above 0.02 s/m$^{1/3}$ would be unrealistic considering the flume material of smooth paintwork. Even a value of 0.05 s/m$^{1/3}$ in the framework of a channel roughness sensitivity

analysis in the FE model leads to minor changes in the discharge split.

Similarly, the influence of wall roughness (Eq. 6) was investigated with the FV model. For test Q300-h50, Table 6 compares values of computed breach discharges with two different wall roughness coefficients (n_w = 0.015 s/m$^{1/3}$ and n_w = 0.030 s/m$^{1/3}$) and without wall roughness. Again, the flow sensitivity was found to be weak, since the relative change in the breach discharge does not exceed 1%. This slight increase in the breach discharge is associated with a change in the velocity profile and unit discharge in the channel immediately downstream of the breach. Figure 12 compares the field of unit discharges obtained without and with wall roughness. The latter is characterized by a wider area of lower velocity close to the right wall, leading to a flow constriction downstream of the breach and, therefore, an increase in the breach discharge.

Table 6 Influence of wall roughness in test Q300-h50 simulated by FV model (algebraic turbulence closure α = 1)

Wall roughness	None	Moderate	High
Coefficient n_w [s/m$^{1/3}$]	0.00	0.015	0.030
Breach discharge [m^3/s]	0.2014	0.2022	0.2035
Relative change [%]		0.4	1.0

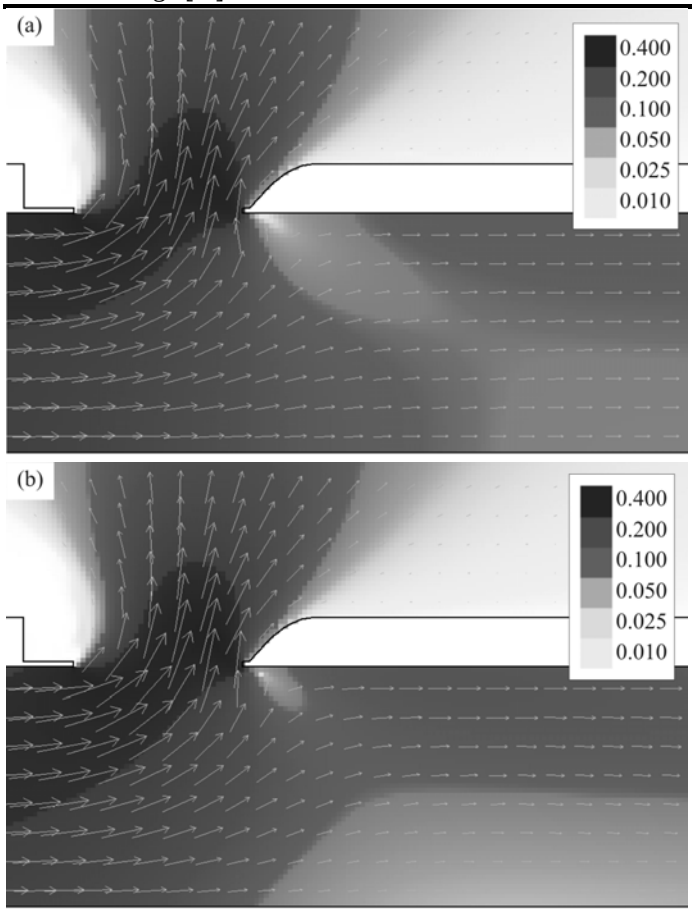

Figure 12 Unit discharges [m^2/s] close to breach location, computed by FV model for test Q300-h50, (a) *without* wall roughness, (b) *with* wall roughness (n_w = 0.030 s/m$^{1/3}$)

5.7 *Influence of Boussinesq coefficients*

Preliminary simulations were run with the FV model considering spatially distributed Boussinesq coefficients (Eq. 5). The upwind scheme described in 4.2 was demonstrated to remain stable regardless of the value of the Boussinesq coefficients (Dewals 2006). The CFL condition however needs to be updated to account for its effect on wave celerity.

Results of these preliminary simulations demonstrate that the Boussinesq coefficients can indeed have a substantial influence on the flow behaviour. These simulations are based mainly on guesses regarding the distribution of the Boussinesq coefficients and must be essentially considered as contributions to a sensitivity analysis of the flow with respect to the Boussinesq coefficients. More realistic simulations can only be executed based on distributions of Boussinesq coefficients inferred from experimental measurements or 3D simulations. In such a framework, the 2D modelling relies on complementary experimental or 3D numerical modelling, which is a weak point of such an approach. However, a detailed analysis of 3D simulation results may lead to a parameterization of the Boussinesq coefficient as a function of depth-averaged flow characteristics (e.g. free surface curvature), which in turn makes the 2D model self-sufficient by adding a closure relationship linking the local Boussinesq coefficient to the primitive unknowns (or their derivative) of the depth averaged model.

Currently, velocity profiles over depth are available from measurements performed at IWW-RWTH for a restricted floodplain area nearby the breach within the body of the wave (2.2). Due to the distribution of horizontal velocity components u and v, the depth averaging yields high values of Boussinesq coefficients, which actually cannot be applied in one-to-one for such heterogeneous profiles.

A simulation with the FV model based simply on this distribution of Boussinesq coefficients indicates a slight increase in the released discharge. Moreover, the real Boussinesq coefficients are expected to differ from unity in a much wider area, including the channel in the breach vicinity. If this overall distribution is taken into account in depth-averaged modelling, the breach discharge might be much more affected. Therefore, 3D simulations are presently undertaken at IWW-RWTH to provide 2D models with a reliable spatial distribution of Boussinesq coefficients in the entire computational domain.

6. Conclusions

Both investigated 2D depth-averaged shallow water models reproduce satisfactorily the basic flow pattern and the qualitative flow split for different configurations of experimental dike-break induced

flows. The flooding event is modelled from an initial state for a closed flap gate in a single stable run, without oscillations including the channel and the wave propagation area. This confirms the convergence and general applicability of the methods used for dike-break problems.

The resulting deviations from the performed measurements including underestimation of breach discharges by 4 to 11% were analysed focusing on the simplifications of the mathematical model and the numerical approach. The applied CFD-methods should at least be of 2nd order accuracy in space to minimize numerical diffusion which otherwise affects the solution. The tested simulations involve a low solution sensitivity as regards turbulence modelling, bed and wall roughness. Accordingly, progress has to be made in the use of Boussinesq coefficients, coupled with experimental and 3D numerical results. Additionally, a non-hydrostatic pressure distribution depending on the free surface curvature should be adopted. Depth-averaging and above all the hydrostatic pressure assumption are reasons for the observed differences between the experimental and numerical investigations of dike-break induced flow.

Acknowledgements

The 2nd author gratefully acknowledges the F.R.S.-FNRS and the University of Liege (ARD and Duesberg Foundation), which provided funding for the numerical research carried out in the framework of his postdoctoral studies at IWW, RWTH Aachen.

The research of the 1st writer was supported by the German Research Foundation (DFG), reference number KO 1573/15-2. The financial support of DFG is gratefully acknowledged.

Notation

a_i coefficients for weir discharge coefficient (i = 0, ... 3)
b crest width
$\mathbf{f}$, $\mathbf{g}$ advective and pressure fluxes
$\mathbf{f}_d$, $\mathbf{g}_d$ diffusive fluxes
F Froude number
g gravitational acceleration
h flow depth
h_o overflow depth
h_w height of weir crest
k degree of polynomial in DG discretization
n_b, n_w bottom and side-wall roughness coefficients
N_x, N_y number of contact edges of finite volume cell
Q_B breach discharge
Q_w weir discharge
$\mathbf{s}$ vector of conservative unknowns
$\mathbf{S}_o$ bottom slope
$\mathbf{S}_f$ friction slope
t time
u depth-averaged velocity component along x-axis
u_* friction velocity
v depth-averaged velocity component along y-axis
$\hat{u}$, $\hat{v}$ components of local velocity
x, y coordinates in horizontal plane
z_b bottom elevation
z vertical coordinate
Δx grid resolution in horizontal plane
Δz grid resolution in vertical plane
α coefficient of turbulent model
μ discharge coefficient
ν_t depth-averaged turbulent eddy viscosity
ν molecular kinematic viscosity
ρ density of water
ρ_{xx}, ρ_{yy}, ρ_{xy} Boussinesq coefficients
σ_x, σ_y turbulent normal stresses
τ_{xy} turbulent shear stress
τ_{bx}, τ_{by} components of bottom shear stress
$\langle\bullet\rangle$ depth-averaged

References

ASCE Task Committee on Turbulence Models in Hydraulic Computations (1988). Turbulence modeling of surface water flow and transport 1. *Journal Hydr. Engng.* 114(9), 970-991.

Aureli, F., Mignosa, P. (2002). Rapidly varying flows due to levee-breaking. Proc. Intl. Conf. *Fluvial Hydraulics* (River Flow), Louvain-la-Neuve, Belgium 1, 459-466.

Aureli, F., Mignosa, P. (2004). Flooding scenarios due to levee breaking in the Po river. *Water Management* 157, 3-12.

Briechle, S., Joeppen, A., Köngeter, J. (2004). Physical model tests for dike-break induced, two-dimensional flood wave propagation. Proc. 2nd Intl. Conf. *Fluvial Hydraulics* (River Flow), Naples, Italy 2, 959-966. Balkema, Rotterdam.

Briechle, S. (2006): Die flächenhafte Ausbreitung der Flutwelle nach Versagen von Hochwasserschutzeinrichtungen an Fließgewässern. Shaker, Aachen [in German].

CADAM (2000). Concerted Action on Dambreak Modelling, *Final Report* SR 571. HR, Wallingford UK.

Choi, S.-U., Garcia, M.H. (2002). k-ε turbulence modelling of density currents developing two dimensionally on a slope. *Journal Hydr. Engng.* 128(1), 55-63.

Cockburn, B. (1999). Discontinuous Galerkin methods for convection-dominated problems. *Lecture Notes in Computational Science and Engineering* 9, 69-224. Springer, Berlin.

Cockburn, B., Karniadakis, G.E., Shu, C.-W. (2000). Discontinuous Galerkin methods. *Lecture Notes in Computational Science and Engineering* 11. Springer, Berlin.

Dewals, B. (2006). Une approche unifiée pour la modélisation d'écoulements à surface libre, de leur effet érosif sur une structure et de leur interaction avec divers constituants. *PhD thesis*. University, Liege [in French].

Dewals, B.J., Erpicum, S., Archambeau, P., Detrembleur, S., Pirotton, M. (2006a). Depth-integrated flow modelling taking into account bottom curvature. *Journal Hydr. Res.* 44(6), 787-795.

Dewals, B.J., Erpicum, S., Archambeau, P., Detrembleur, S., Pirotton, M. (2006b). Numerical tools for dam break risk assessment: Validation and application to a large complex of dams. *Improvements in reservoir construction, operation and maintenance*, 272-282. H. Hewlett, ed. Telford, London.

Dewals, B.J., Kantoush, S.A., Erpicum, S., Pirotton, M., Schleiss, A.J. (2008). Experimental and numerical analysis of flow instabilities in rectangular shallow basins. *Environ. Fluid Mech.* 8, 31-54.

Erpicum, S. (2006). Optimisation objective de paramètres en écoulements turbulents à surface libre sur maillage multibloc. *PhD Thesis*. University, Liege [in French].

Erpicum, S., Archambeau, P., Detrembleur, S., Dewals, B., Pirotton, M. (2007). A 2D finite volume multiblock flow solver applied to flood extension forecasting. *Numerical modelling of hydrodynamics for water resources* 321-325, P. García-Navarro, E. Playán, eds. Taylor & Francis, London.

Ferziger, J.H., Peric, M. (1996). Further discussion of numerical errors in CFD. *Int. Journal Num. Meth. in Fluids* 23, 1263-1274.

Ferziger, J.H., Peric, M. (2002). *Computational methods for fluid dynamics*. Springer, Berlin.

Fischer, H., List, E., Koh, R., Imberger, J., Brooks, N. (1979). *Mixing in inland and coastal waters*. Academic Press, New York.

Fraccarollo, L., Toro, E. (1995). Experimental and numerical assessment of the shallow water model for two-dimensional dam-break type problems. *Journal Hydr. Res.* 33(6), 843-863.

Ghamry, H.K., Steffler, P.M. (2002). Two dimensional vertically averaged and moment equations for rapidly varied flows. *Journal Hydr. Res.* 40(5), 579-587.

IMPACT (2005). Investigation of extreme flood processes and uncertainty. *Final Technical Report* EVG1-CT-2001-00037. HR Wallingford UK.

Kulisch, H. (2003). *Ausbreitung von Dammbruchwellen im physikalischen Modell.* Oldenbourg, München [in German].

Rodi, W. (1984). *Turbulence models and their application in hydraulics*: A state-of-the-art (2nd ed.). Balkema, Rotterdam.

Schwanenberg, D., Köngeter, J. (2000). A discontinuous Galerkin method for the shallow water equations with source terms. *Lecture Notes in Computational Science and Engineering* 11, 419-424. Springer, Berlin.

Schwanenberg, D., Harms, M. (2002). Discontinuous Galerkin method for dam-break flows. Proc. Intl. Conf. *Fluvial Hydraulics* (River Flow), Louvain-la-Neuve, Belgium 1, 443-448.

Schwanenberg, D. (2003). *Die Runge-Kutta-Discontinuous-Galerkin-Methode zur Lösung konvektions-dominierter tiefengemittelter Flachwasserprobleme.* Shaker, Aachen [in German].

Schwanenberg, D., Harms, M. (2004). Discontinuous Galerkin Finite-Element Method for transcritical two-dimensional shallow water flows. *Journal Hydr. Engng.* 130(5), 412-421.

Shu, C.-W. (2003). High order finite difference and finite volume WENO schemes and discontinuous Galerkin methods for CFD. *Int. Journal Comput. Fluid Dyn.* 17, 107-118.

Younus, M., Chaudhry, M.H. (1994). A depth-averaged k-ε turbulence model for the computation of free-surface flow. *Journal Hydr. Res.* 32(3), 415-439.